

TUMSAT-OACIS Repository - Tokyo

University of Marine Science and Technology

(東京海洋大学)

Observation of Wetting Behavior with Ultralow Contact Angle by a Total Reflection and Interference Fringe Method

メタデータ	言語: eng 出版者: 公開日: 2022-03-08 キーワード (Ja): キーワード (En): 作成者: Li, He, Tanaka, Kentaro, Iwamoto, Katsumi メールアドレス: 所属:
URL	https://oacis.repo.nii.ac.jp/records/2319

This work is licensed under a Creative Commons Attribution-NonCommercial-ShareAlike 3.0 International License.



Observation of wetting behavior with ultra-low contact angle by a total reflection and interference fringe method

AUTHOR NAMES

He Li, Kentaro Tanaka, Katsumi Iwamoto*

AUTHOR ADDRESS

He Li — Graduate School of Marine Science and Technology, Tokyo University of Marine Science and Technology, 2-1-6, Etchujima, Koto-ku, Tokyo 135-8533, Japan

Kentaro Tanaka — Department of Marine Electronics and Mechanical Engineering, Tokyo University of Marine Science and Technology, 2-1-6, Etchujima, Koto-ku, Tokyo 135-8533, Japan

Katsumi Iwamoto — Department of Marine Electronics and Mechanical Engineering, Tokyo University of Marine Science and Technology, 2-1-6, Etchujima, Koto-ku, Tokyo 135-8533, Japan

KEYWORDS

wetting, super-hydrophilicity, super-oleophilicity, contact angle, contact line, fringe method

ABSTRACT

In order to study the wetting behavior of a liquid film on a surface with ultra-low contact angle, the interference fringe method with oblique upward laser is developed. This method allows to detect the position of contact line precisely and observe the surface profile of very thin film. The contact angle measurement is verified within from 0.007° to 3° . The wetting behavior of silicone oil droplet on a glass substrate is observed. The wetting process can be distinguished with three stages, such as advancing, stable and receding stage. In the stable stage, there are two angles near the contact line. And the two angles have opposite variations in trend. It can be seen that there are some reciprocating changes in the two angles and the thickness of the liquid film near the contact line during the stable stage, like the edge of the surf.

INTRODUCTION

When a droplet is placed on a substrate, wetting behavior will occur. No matter in natural systems or man-made systems, wetting behavior is important in large scale and small scale. For example, in oil recovery,¹ coating,² friction,^{3,4} printed electronics⁵ and printing,^{6,7} hydrophobicity/oleophobicity and hydrophilicity/oleophilicity play significant roles. The superhydrophilicity is desirable for self-cleaning and antireflective coatings applied in glasses, flexible electronics, and solar cells protective panels.^{8,9} In particular, in the printed electronics technology, high-definition thin film patterns such as semiconductors and metals are formed using printing technology for drawing characters and photographs, and these are combined to manufacture electronic devices, and in the process it requires ink droplets mixed with other materials. But there

are some unclear problems on the thin film growth occurs near the surface of the ink droplet. And it is also a subject to be solved that whether such thin film growth is possible for various ink combinations. So that, measurement and observation for the wettability and wetting behavior of the inks which have super-hydrophilicity/super-oleophilicity is necessary. Since the tendency for the liquid to spread has relation to contact angle. Hence, the contact angle is a useful measure of wettability.¹⁰ The contact angle located at contact line (C.L.), is the angle formed by the liquid-gas interface and the solid or immiscible liquid surface.¹¹ The C.L., defined to be the locus of points that are simultaneously in contact with the gas, liquid and solid phases.¹²

There are some methods applied to measure the contact angle. One of the most common methods is the side view method.¹³⁻¹⁶ This method can be used to measure the contact angle with an accuracy $\pm 1^\circ \sim 2^\circ$,¹⁷ however, it is difficult to determine the position of the C.L. precisely, especially in super-hydrophilic/super-oleophilic surface with very small contact angle. For measuring small contact angles, the reflection of a laser beam method can be used for measuring contact angle $\theta > 4^\circ$ with an accuracy of $\pm 0.5^\circ$,¹⁸ and the interferential reflection contrast microscopy (IRCM) method can be used for measuring contact angle $1^\circ < \theta < 4^\circ$ with an accuracy of $\pm 0.01^\circ$.¹⁹ IRCM is known as a fringe method. With the fringe method, the contact angle and surface profiles of alcohol droplets^{20,21}, silicone oil droplets²² and water droplets²³ can be measured. When the thickness of the film is tens micrometer or even nanometer, the Brewster angle microscope can be used to observe it.^{24,25} Contact angle and the C.L. can also be observed simultaneously. But there is a problem when the liquid is located between two planes that have a narrow gap or when an object on the liquid,^{15,25} observation cannot be performed because the light for interfering is blocked. Although the film trapping technique (FTT) can be used to measure the contact angle when micrometer particles on the liquid, the measurement accuracy of FTT is

$\pm 2^\circ \sim 5^\circ$,²⁶ which is obviously difficult to measure the small contact angle on super-hydrophilic/super-oleophilic surfaces. In our experiment, the fringe method with oblique upward laser is developed. The contact angle and surface profile could be evaluated by observing interference fringes. At the same time, the C.L. can also be determined.

EXPERIMENTAL SECTION

Experimental principle. In this experiment, the laser enters from bottom to the observation plane. By setting the incident angle that yields total reflection at solid-gas interface and partial refraction at solid-liquid interface, the wetting and non-wetting area can be distinguished clearly. So that, the C.L. can be determined. And incident laser which reflected at liquid-air interface generates an interference fringe pattern which corresponds to the surface profile of the liquid.

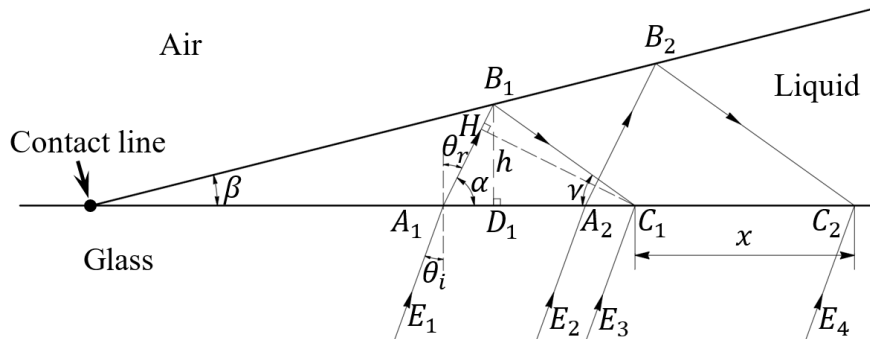


Figure 1. Schematic diagram of relationship between spacing of interference fringe and contact angle. The droplet is placed on the glass substrate and forms a liquid film with a contact angle of β . The fringe at point C_1 is the interference fringe closest to the contact line. The contact angle β equals the inclination angle of the line where the reflection points B_1 and B_2 are located. θ_i is the angle of incidence and θ_r is the angle of refraction. Angle α and γ are the angles between light E_1 and the liquid-glass interface.

When a droplet is placed on a glass substrate and forms a liquid film, if only the surface profile of the liquid film near the C.L. is concerned, the curve at the air-liquid interface can be approximated as a straight line. Figure 1 schematically shows the profile of liquid film near the C.L. on the glass substrate, for which the contact angle is β . Light E_1 enters and refracts at point A_1 on the liquid-glass interface with incident angle θ_i and penetrates into the liquid, and then reflects at point B_1 on the air-liquid interface, finally, refracts at point C_1 on the liquid-glass interface. Coherent light E_3 intersects light E_1 at point C_1 . The point H on light E_1 and point C_1 on light E_3 have same phase. $HB_1 + B_1C_1 = L_1$ is the optical path difference between reflected light of E_1 and light E_3 at point C_1 . When the phase difference between the lights is an even multiple of π , constructive interference occurs, and the intensity of the interferogram is strong (light fringe). Similarly, when the phase difference is an odd multiple of π , destructive interference occurs, and the intensity of the interferogram is weak (dark fringe).²⁷ The optical path difference of one wavelength corresponds to one phase difference of 2π .

The condition of first dark fringe is: phase difference = π , $L_1 = \lambda$. Where λ is the wavelength of light in liquid. Similarly, L_2 is the optical path difference corresponding to the second dark fringe, then the difference between L_1 and L_2 is λ . x is the distance between the two adjacent dark fringes. (the distance between two adjacent light fringes also equals to x , and here we just use dark fringes.)

An equation about contact angle β and x can be derived:

$$x = \frac{\lambda \cos \gamma (\tan \gamma \pm \tan \beta)}{[1 - \cos(\alpha + \gamma)] \tan \beta} \quad (1)$$

With eq (1), the contact angle β can be calculated. When calculating the contact angle at left side of the droplet (as shown in Figure 2), the upper “+” of plus-minus sign in eq (1) is used.

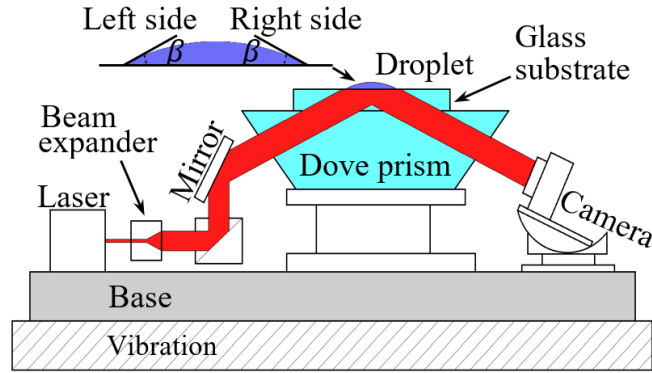


Figure 2. Schematic diagram of experimental apparatus. The experimental device is located on the vibration isolator. The red laser enters from one side of dove prism through a beam expander. Images including interference fringes were taken by the camera.

Facilities and materials. The schematic diagram of experiment apparatus is shown in Figure 2. The test liquid in this experiment is silicone oil (Shin-Etsu Chemical Co., KF-96L-1CS). According to the technical data, the refractive index of silicone oil is 1.382 (25°C)²⁸. The silicone oil droplet has a volume of 1 μ L, a density of $\rho = 818\text{kg m}^{-3}$, a surface tension of $\sigma = 16.9\text{mN m}^{-1}$ and a kinematic viscosity of $\nu = 1\text{mm}^2\text{s}^{-1}$ (25°C)²⁸. The silicone oil droplet is placed on a glass substrate (MATSUNAMI MAS-GP S9902) with surface roughness $Ra = 0.006\mu\text{m}$ by a micropipette (NICHIRYO Nichipet EX 0.5-10 μ L). The glass substrate is set on the dove prism (Thorlabs PS995 N-BK7). To eliminate the effect of the gap between the glass substrate and the dove prism, the gap is filled with cedar oil (FUJIFILM Wako chemicals 8000-27-9), which has an almost same refractive index with glass.²⁹

Camera (Nikon Nikon1V3 18.39million pixels, CMOS captures images in 24-bit RGB format with resolution 2.5 μm /pixel) observes the interference fringes from one side of the dove prism. The laser (Thorlabs HNL100L-JP, wavelength: 632.8nm) is set on the other side.

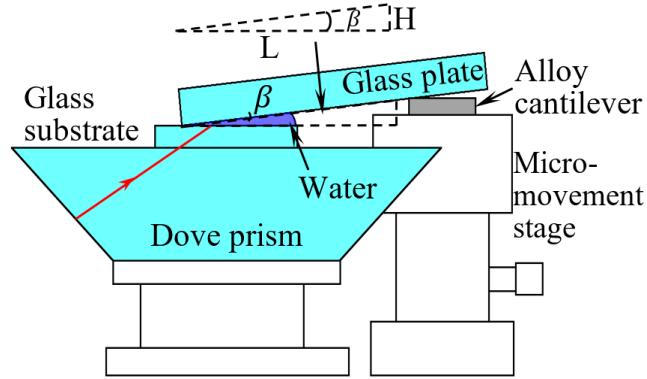


Figure 3. Schematic diagram of experimental apparatus of verification. The micro-movement stage controls the inclination angle of the glass plate. The wedge region formed by the glass plate and the glass substrate is filled with water.

Verification experiment. In order to verify the correctness of eq (1), a verification experiment was performed. The schematic diagram of verification experiment apparatus is shown in Figure 3. In this experiment, contact angle β equals the angle of inclination of the glass plate. The length of horizontal side of contact angle β is L and the length of vertical side which opposites to contact angle β is H . Contact angle β can be calculated with L and H , easily. The glass plate is used as the hypotenuse of a triangle, and metal alloy cantilever is used to up and down along the vertical line to tilt the glass plate. Water is injected between the glass plate and the glass substrate. The glass substrate was placed on the dove prism so that the angle could be changed from 0° .

In order to control the contact angle β , a micro-movement stage (Sigmakoki TSD-603) with an adjustment knob is used. When the knob rotates one turn, it moves up or down by 0.5 mm. There are 50 marks on one turn of the knob, and two rounds are 1 mm, hence, the adjustment accuracy of the stage is under 0.01 mm.

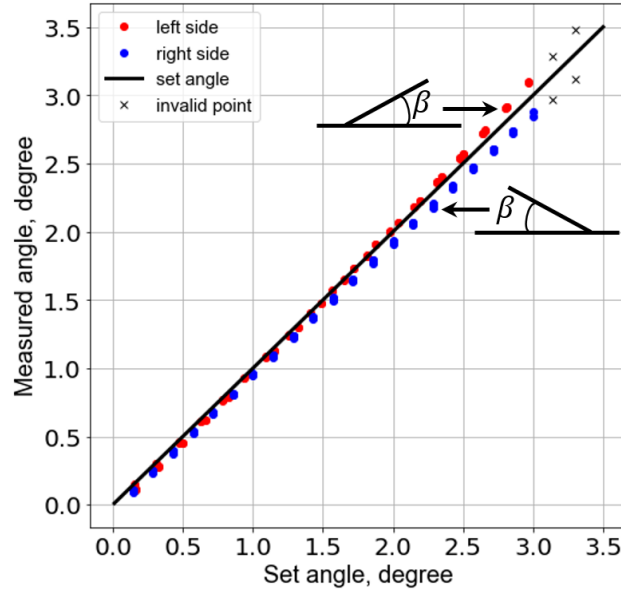


Figure 4. Result of verification experiment. In this figure, the red dots indicate the measured value on the left side of the droplet, and the blue dots indicate the value on the right side of the droplet. When the contact angle is bigger than 3° , the interference fringe becomes blurred and cannot be distinguished.

Turn the knob to make the metal alloy cantilever rise at 0.05mm every time. During this process, images of fringes are taken by the camera. When the contact angle was located on the left side and right side, the experiment was performed 4 times respectively. The experimental result is shown in Figure 4. The measured angle from the interference method is in good agreement with the set angle. An obvious trend can be seen: as the contact angle becomes larger, the error becomes larger. According to the results of eight times' experiments, the minimum measurable angle is 0.007° . When the contact angle is between 0.5° and 3° , the error percentage is $\pm 6\%$. From 0.5° to 0.2° , there is a linear increase in the error percentage from $\pm 6\%$ to $\pm 10\%$. And the error percentage from 0.2° to 0.007° is $\pm 10\%$. Thus, it is confirmed that the equation and observation method of this experiment can be used to measure the contact angle when the contact angle is smaller than 3° .

Calculation of the surface profile. There are some reflection points which are corresponding to interference fringes, on the air-liquid interface. Before calculating the surface profile of a liquid, the horizontal and vertical positions of the reflection points need to be calculated first. Then connect these reflection points with curves to get the surface profile of the liquid. In the verification experiment, because the surface of the inclined glass plate is a plane, the angles corresponding to all interference fringes are the same. It is easy to calculate all the horizontal and vertical positions of the reflection points without a large cumulative error.

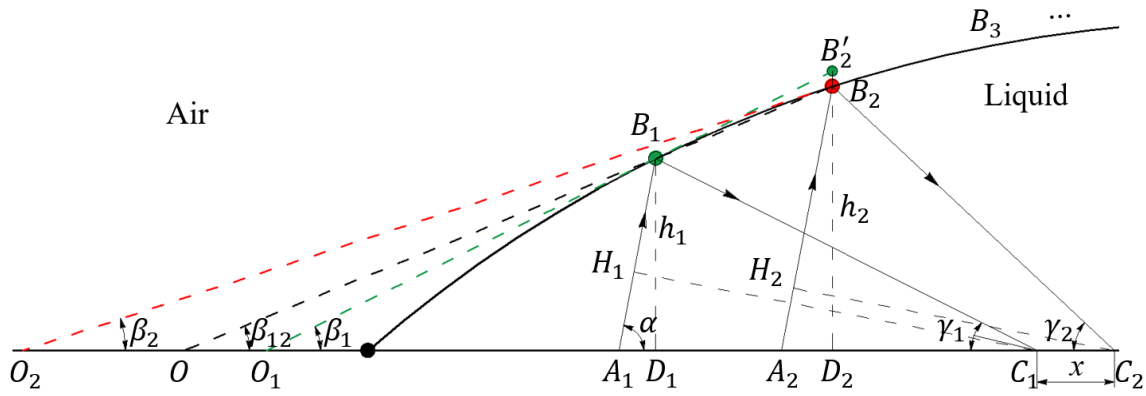


Figure 5. Image of the surface profile of a liquid film. Line B_1O_1 is a tangent line passing through point B_1 , line B_2O_2 is a tangent line passing through point B_2 , and the corresponding inclination angles of these two lines are β_1 and β_2 . And β_{12} is the inclination angle of line B_1B_2 . The surface profile of the liquid is composed of line segments such as B_1B_2 and B_2B_3 .

However, the surface profile of the liquid film is not a plane, as shown in Figure 5. The tangent line at point B_1 is B_1O_1 and the tangent line at point B_2 is B_2O_2 , and the inclination angles are β_1 and β_2 , respectively. The angle between the reflected light B_2C_2 and substrate OC_2 is $\gamma_2 = \alpha - 2\beta_2$. At this moment, if the angle β_1 and the height h_1 of the point B_1 are used to calculate the height h_2 of point B_2 , the calculated height will be the height of B'_2 . As shown in Figure 5, the point B'_2 is higher than point B_2 . If the subsequent points are also calculated accordingly, the final

calculated result is bound to a large error. To reduce this cumulative error, we connect points B_1 and B_2 to form a line segment B_1B_2 . B_1O is its extension line, and angle β_{12} is its inclination angle. If it is assumed that the curve between point B_1 and point B_2 is part of a circle, then $\beta_{12} = (\beta_1 + \beta_2)/2$. Similarly, the inclination angles of the next segments can be obtained by the same method. With these corrected inclination angles, the horizontal and vertical positions of the reflection points at the air-liquid interface can be calculated.

x is the distance between the two adjacent dark fringes, and λ is the wavelength of laser in the liquid. From Figure 5, we can get geometric relationships about x and λ : $D_2C_2 + D_1D_2 - D_1C_1 = x$ and $A_2B_2 + B_2C_2 - A_2H_2 - (A_1B_1 + B_1C_1 - A_1H_1) = \lambda$. The specific equations are shown below:

$$h_2 \cot \gamma_2 + (h_2 - h_1) \cot \beta_{12} - h_1 \cot \gamma_1 = x \quad (2)$$

$$h_2 \left(\sin \alpha + \frac{1}{\sin \gamma_2} - \cot \gamma_2 \cos \alpha \right) - h_1 \left(\sin \alpha + \frac{1}{\sin \gamma_1} - \cot \gamma_1 \cos \alpha \right) = \lambda \quad (3)$$

h_1 can be calculated by the condition of the optical path difference $L = \lambda$. With eq (2) and (3), h_2 can be represented by x , h_1 and β_{12} :

$$h_2 = \frac{x \pm h_1 \cot \gamma_1 + h_1 \cot \beta_{12}}{\cot \beta_{12} \pm \cot \gamma_2} \quad (4)$$

With eq (2) and (3), an equation about β_{12} and x can be derived:

$$x = \frac{\left[h_1 \left(\sin \alpha + \frac{1}{\sin \gamma_1} - \cot \gamma_1 \cos \alpha \right) + \lambda \right] (\cot \beta_{12} \pm \cot \gamma_2)}{\left(\sin \alpha + \frac{1}{\sin \gamma_2} - \cot \gamma_2 \cos \alpha \right) (h_1 \cot \beta_{12} \pm h_1 \cot \gamma_1)} \quad (5)$$

In eq (4) and (5), when calculating the angles at left side of the liquid film, $\gamma_1 = \alpha - 2\beta_1$, $\gamma_2 = \alpha - 2\beta_2$, and the upper “+” before $\cot \gamma_2$ and $h_1 \cot \gamma_1$ are used. Convergence calculation is performed by using eq (5) with a calculation accuracy of 1/1000 of x , and β_{12} can be obtained. And the angles for next segments can be obtained in the same manner. Then we can calculate all the horizontal and vertical positions of the reflection points.

Since the interference of light requires at least one wavelength in optical path difference, there is a minimum film thickness that can be measurable. The minimum measurable thickness changes in the range of 200 nm to 600 nm according to the incident angle θ_i (as shown in Figure 1).

Experiment procedures. The silicone oil is deposited on the horizontal surface of glass substrate by the micropipette through a needle and then forms a liquid film immediately. To reduce the impact of the droplet from the tip of the micropipette to the glass substrate, the tip of the micropipette is in contact with the glass substrate when the droplet is placed. Experiments were performed under $18\pm 0.5^\circ\text{C}$ room temperature and $46\%\pm 2\%$ of relative humidity. The capillary length under this condition is $l_c = 1.45\text{mm}$.

The material of dove prism and glass substrate is BK7, and the refractive index of BK7 is 1.517. From Snell's law, we can know that the ratio of phase velocities in two media is equal to ratio of sine of incident angle θ_i in one media and sine of refraction angle θ_r in the other media.³⁰ So the critical angle of total reflection between glass substrate and air is 41.2° and the critical angle of total reflection between glass substrate and silicone oil is 65.6° . The middle value of the two critical angles is 53.5° . Taking liquids with higher refractive index into account, the incident angle θ_i is set between 48.3° and 53.5° , in which the reflection of non-wetting area is total reflection, and the reflection of wetting area is partial reflection. In this experiment, the incident angle θ_i is 50.3° . Before each new experiment, the glass substrate is replaced with a new one. Under the same conditions, the experiment was performed five times. The results of these five experiments showed the similar trend. In addition, we also used acetone-cleaned glass plates for experiments, and the experimental results are in good agreement with the results of using new glass plates. The treatment of the acetone-cleaned glass plate is as follows: the glass substrate is put inside an ultrasonic washing machine in purified water to eliminate dusts and fats on the surface of the glass substrate

for 10min, then, the glass substrate is put in acetone and washed by the ultrasonic washing machine for 10min to eliminate tiny contamination. Then the glass substrate is washed by using distilled water to eliminate acetone that is remained on the surface. Finally, the clean glass substrate is subsequently dried in a vacuum oven at 70°C for 30min, at the end of which the glass substrate is allowed to cool under vacuum.

During the wetting process, the C.L. and the interference fringes formed by the surface shape of the liquid film are recorded by the camera with a frame rate of 30 f.p.s.. When observing the wetting behavior of silicone oil, the observed spreading time of the liquid is greater than 100 s.

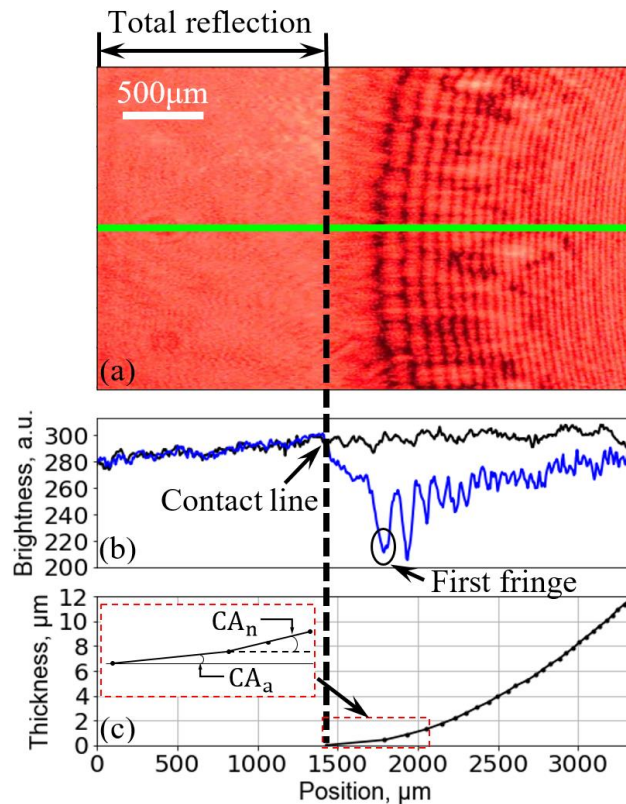


Figure 6. A snapshot of interference fringes of the liquid film formed by silicone oil droplet in the wetting process. The black vertical dotted line is located at the position of the contact line in Figure 6 (a), (b) and (c). In Figure 6 (a), the green horizontal line indicates the analyzing line. The black curve in Figure 6 (b) indicates the brightness of the reflected light when the droplet is unplaced.

The blue curve indicates the brightness of the reflected light with the droplet. In Figure 6 (c), the black curve indicates the calculated surface profile of the droplet, and the red dotted rectangular part is an illustration of CA_a and CA_n .

RESULTS AND DISCUSSION

The wetting experiment of silicone oil droplet is observed by our interference fringe method. Figure 6 shows the typical interference fringe, brightness curve and calculated surface profile of the liquid film. Figure 6 (b) shows the brightness-position curve. Due to the total reflection area and partial reflection area, it is easy to determine the position of the C.L. from the brightness-position curve. The first fringe is the first dark fringe adjacent to the C.L.. As shown in Figure 6 (a), when reading the brightness along the green line, if the reading width is only 1 pixel, there will be a lot of noise on the peak value of the read brightness. Adjust the reading width to get the spatial average with 20 pixels ($50\ \mu\text{m}$), in which condition, there will be much less noise while the brightness value can also be read clearly. However, it is still impossible to easily determine the specific location of the brightness peak. Since the distance between adjacent dark fringes is longer than $40\ \mu\text{m}$, to reduce noise, we choose a low-pass filter to filter the wavelength which is shorter than $40\ \mu\text{m}$. According to the processed graphics, the brightness peak values can be found quickly, thereby the x can be measured. With x , the surface profile of the liquid film can be calculated by using eq (5) (as shown in Figure 6 (c)). Figure 7 shows the surface profiles which are calculated by this method at four moments during the wetting process. According to the surface tension, the curvature of a part of the surface profile can be approximated as an arc. Take two points which are closest to the center on the calculated profiles of left and right side and take another point which

is near one of the two points to determine a circle. The same operation is repeated ten times to obtain ten circles, and the radii of these ten circles are averaged to obtain the radius of the fitted circle. In Figure 7, the dashed lines represent parts of the fitted circles. The thickest part of the liquid film is around $20\mu\text{m}$. With the passage of time, the wetting diameter is constantly changing. At the same time, the thickness of the liquid film is getting thinner and the total volume continues decreasing due to evaporation. The volume of the liquid film through the obtained surface profile can be calculated, thereby the average evaporation rate can be obtained. In this experiment, the calculated average evaporation rate of the silicone oil is $1.44 \times 10^{-5} \mu\text{L}/(\text{s} \cdot \text{mm}^2)$.

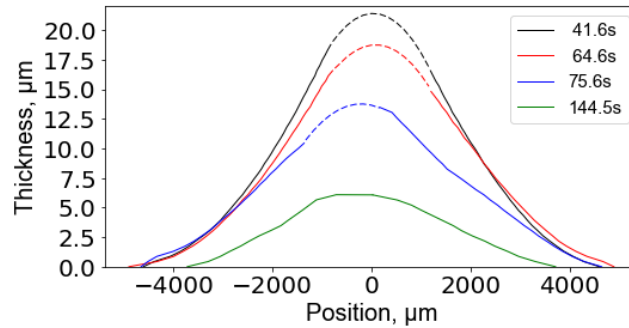


Figure 7. Surface profiles of the liquid film at four moments. In this figure, the solid line parts are calculated from interference fringes, and the dash line parts are fitted with a circle.

By observing the wetting process, around the C.L., different area has different trend that is found. The angle between the first fringe and C.L. has some relatively large reciprocating changes, while the angle between the first fringe and the third fringe has some relatively small reciprocating changes. The third fringe to the fourth fringe or to the further fringe that approach to the center of the film, the angle hardly has reciprocating changes. In the experiment, when measuring the contact angle, there are two angles around the C.L. can be used to characterize the process of wetting. In this study, CA_a represents the angle between the first fringe and C.L., and CA_n represents the angle between the first fringe and the third fringe. As shown in Figure 6 (c), in the

same cross section, connect the point of the C.L. and the reflection point of the first fringe to form a line segment. The CA_a is the inclination angle of this line segment. From the geometric relationship about the spacing between the C.L. and the first fringe (L_{CF}) and CA_a in Figure 6 (c), we can know that L_{CF} and CA_a are negatively correlated. Figure 8 indicates the relationship about position of the C.L. and the first fringe, the CA_a and the CA_n in the wetting process. However, as Figure 8 (b) and (c) indicate, the CA_a and the CA_n show opposite trends. As Figure 8 (a) shows, before advancing of the C.L. stops, the liquid spreads out quickly until at 64 s. At about 125 s, the C.L. cannot be kept in the range of the positions in the past 61 s and starts to recede. During the wetting process, for the C.L., there are three stages can be found. They are advancing, stable and receding stage, respectively. As shown in Figure 8 (a), in the advancing stage, the C.L. keeps advancing, and there is no big fluctuations in the L_{CF} . In the same time, as Figure 8 (b) and (c) shows, the CA_a shows an increasing trend, while the CA_n shows a decreasing trend. When entering the stable stage, the position of the C.L. does not change significantly. However there are some big fluctuations in the first fringe, which leads some fluctuations in L_{CF} . Both of the CA_a and CA_n do not change monotonously and begin reciprocating changes. The fluctuations of the CA_a and CA_n are about 0.1° and 0.03° , respectively. The changes are sharp. The sharp receding of the first fringe corresponds to the sharp decreasing of the CA_a . And the sharp advancing of the first fringe corresponds to the sharp increasing of the CA_a . For the CA_n , the corresponding situation of change is opposite. For the receding stage, the C.L. recedes continually and there are no big fluctuations in the CA_a .

For the reciprocating changes of contact angles, evaporation is an important factor that has to be considered. From the profiles shown in Figure 7, the liquid has been evaporating. Since the

liquid film near the C.L. is very thin, a small amount of evaporation will affect the contact angle. As the liquid film becomes thinner, the CA_a also becomes smaller. According to Young's equation, when the contact angle of a liquid initially in equilibrium becomes smaller, the combined force of the liquid surface tension and the solid-liquid interfacial tension will be greater than the solid-gas interfacial tension. However, since the CA_n becomes bigger, the Laplace pressure at the reflective surface of the first fringe gets bigger. When the C.L. tends to move to return to the equilibrium state, the liquid at the reflective surface of the first fringe will also tend to flow to return to the equilibrium state. But due to the difference in liquidity, the liquid at the reflective surface of the first fringe completed the flow faster. The repetition of this process forms the phenomenon of reciprocating changes in the contact angles.

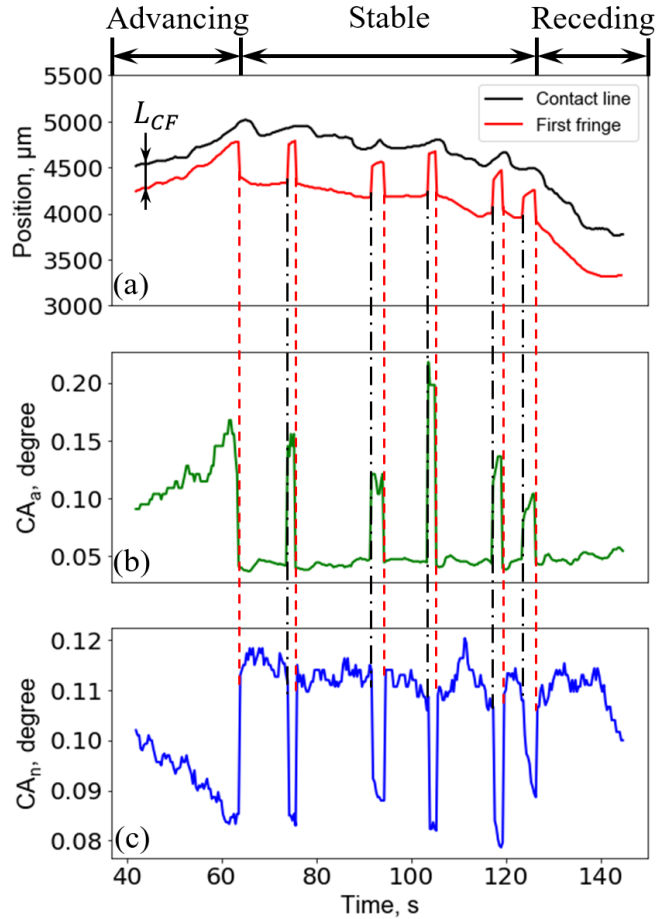


Figure 8. Relationship about position of the C.L. and the first fringe, the CA_a and the CA_n . In Figure 8 (a), the black curve indicates the position of the C.L. and the red curve indicates the position of the first fringe. In this figure, the red vertical dashed lines indicate the moments when the position of the first fringe recede sharply. And the black vertical dashed-dotted lines indicate the moments when the position of the first fringe advance sharply.

In Figure 9 (a), 1 to 9 indicate nine moments in the wetting process. (In Figure 9 (a), between moments 4 and 5, there are 60 frames of picture. For the observation of wetting behavior, the speed of 30 f.p.s. is sufficient.) The surface profiles of the liquid film near the C.L. at these nine moments are shown in Figure 9 (b), (c) and (d). Among the nine moments, 1 and 2 are in the advancing stage. The moment of 2 is also the start of the stable stage. And 3 to 7 are in the stable stage. As

shown in Figure 9 (a), the L_{CF} at the moment of 5 is shorter than it at the moment of 4 and 6. Profiles in Figure 10 are partial enlarged drawing of the profiles at the moments of 4 to 6 near the C.L.. The profile at the moments of 4 and 6 almost overlap. In this figure, the CA_a is the inclination angle of the part indicated by the blue double arrow, and the CA_n is the inclination angle of the part indicated by the black double arrow. When the liquid film has a shorter L_{CF} , the liquid film is thicker, and has a bigger CA_a and a smaller CA_n than the liquid film with a bigger L_{CF} . There are some processes of reciprocating change in thickness, CA_a and CA_n when profiles change from 2 to 7 in the stable stage (as shown in Figure 8 and Figure 9). It can be seen that the reciprocating changes in the two contact angles and the thickness of the liquid film near the C.L., like the edge of the surf. The moment of 8 is the end of the stable stage, as shown in Figure 9 (a), and it is also the end of the reciprocating changes.

According to the experiments we have done, under the same experimental conditions and using the glass substrate of the same product, decane and octane also show similar fluctuations to the silicone oil in contact angles.

In addition, the presence of the very thin liquid film near the C.L. reminds us of the precursor film. According to the previous studies about the precursor film, the length of the precursor film is time-dependent, and the film thickness is a few Å to a few μm .³¹⁻³³ And the inflection point can be found at the junction of the precursor film region and the outer macroscopic region to determine the small apparent contact angles.³⁴ In this experiment, the thickness of the liquid film on the μm scale was observed, and the length of the part whose thickness was less than a few μm was not related to time. Because the thickness of the liquid film is within about 20 μm , the liquid film does not show an obvious inflection point to determine the apparent contact angle. The information

obtained from this study is not sufficient to determine whether the measured liquid film is a precursor film or not.

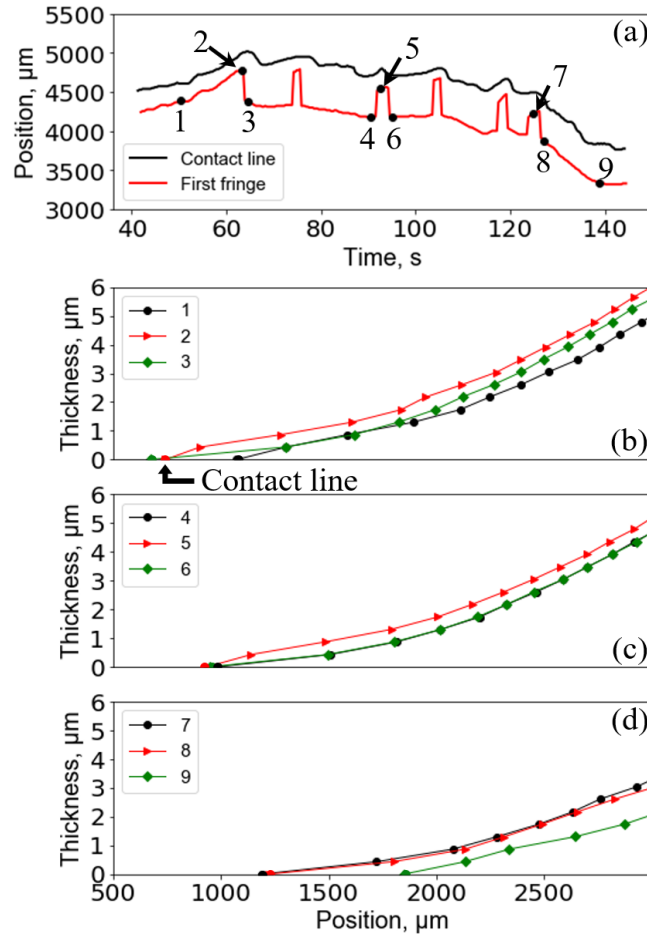


Figure 9. Surface profiles of the liquid film near the C.L.. 1 to 9 in Figure 9 (a) indicate the nine moments in the wetting process. The surface profiles of the liquid film near the C.L. at the nine moments are shown in Figure 9 (b), (c) and (d).

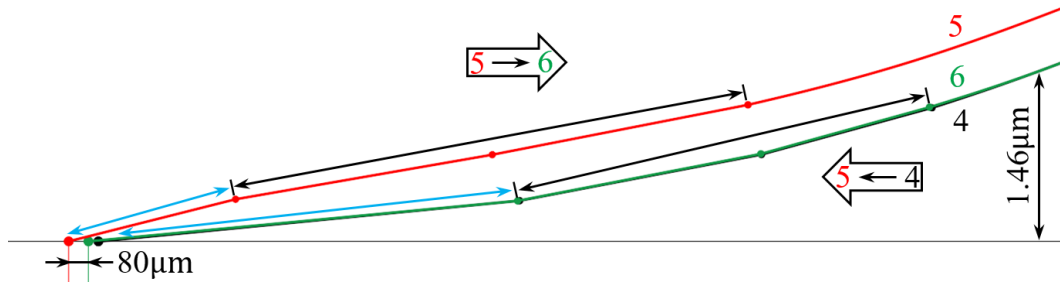


Figure 10. Partial enlarged drawing of the profiles at the moments of 4 to 6 near the C.L.. Profile changes from moment 4 to 5, and then changes to moment 6, while the contact line moves $80\mu\text{m}$. The profile at the moments of 4 and 6 almost overlap.

CONCLUSIONS

In order to measure the contact angle and the position of the contact line of the liquid film simultaneously, an interference fringe method with oblique upward laser is developed. In the wetting experiment, by setting the incident angle of laser, so that the non-wetting part has total reflection and wetting part has partial reflection. As a result, the position of the contact line can be determined. The contact angles and profile of liquid film can be calculated by the derived equations with the spacing of the fringes. The equation is confirmed by verification experiment. And the verified minimum measurable angle is 0.007° . When the contact angle is between 0.007° and 3° , this method can be accurately used for measurement.

The wetting behavior of a liquid film on a surface with ultra-low contact angle is observed by this interference fringe method. According to the results of the wetting experiment, position of the contact line, the surface profile of the liquid film and the contact angles can be observed simultaneously. While, when measuring the contact angle, two contact angles are measured. And the two contact angles have opposite trends. In addition, there are three stages occurred in the wetting process. They are advancing, stable and receding stage. In the first stage, the position of

the contact line continues advancing. And both contact angles have a monotonous change. In the second stage, the position of the contact line does not change significantly, while there are some fluctuations in the L_{CF} . That is caused by reciprocating changes in the CA_a . In the third stage, the position of the contact line is receding and the contact angles have no reciprocating changes. The advancing contact angle is often larger than the receding contact angle in the wetting process.^{11,35} In this experiment, the CA_a is constantly increasing in the advancing stage, however remains unchanged in the receding stage, and the CA_a in the advancing stage is larger than it in the receding stage. For the CA_n , in the first half of the receding stage, the CA_n keeps unchanged, and in the latter half of the stage, the CA_n rapidly decreases. And the CA_n in the advancing stage is smaller than it in the receding stage.

AUTHOR INFORMATION

Corresponding Author

Kentaro Tanaka — Department of Marine Electronics and Mechanical Engineering, Tokyo University of Marine Science and Technology, 2-1-6, Etchujima, Koto-ku, Tokyo 135-8533, Japan; orcid.org/0000-0002-2880-9923; Email: kentaro@kaiyodai.ac.jp

Notes

The authors declare no competing financial interest.

ACKNOWLEDGMENT

This work was supported by JSPS KAKENHI Grant Number 15562555.

REFERENCES

- (1) Bertrand, E.; Bonn, D.; Broseta, D.; Dobbs, H.; Indekeu, J.; Ragil, K.; Shahidzadeh, N. Wetting of alkanes on water. *Journal of Petroleum Science and Engineering* **2002**, 33, 217-222.
- (2) Bonn, D.; Eggers, J.; Indekeu, J.; Meunier, J.; Rolley, E. Wetting and spreading. *Reviews of Modern Physics* **2009**, 81, 739-805.
- (3) Klein, J.; Perahia, D.; Warburg, S. Forces between polymer-bearing surfaces undergoing shear. *Nature* **1991**, 352, 143-145.
- (4) Guo, F.; Li, X. M.; Wong, P. L. A novel approach to measure slip-length of thin lubricant films under high pressures. *Tribology International* **2012**, 46, 22-29.
- (5) Liu, X. Y.; Kanehara, M.; Liu, C.; Sakamoto, K.; Yasuda, T.; Takeya, J.; Minari, T. Spontaneous patterning of high-resolution electronics via parallel vacuum ultraviolet. *Advanced Materials* **2016**, 28, 6568-6573.
- (6) Yoon, H.S.; Lee, H.T.; Kim, E.S.; Ahn, S.H. Direct printing of anisotropic wetting patterns using aerodynamically focused nanoparticle (AFN) printing. *Applied Surface Science* **2017**, 396, 1450-1457.
- (7) Liu, F.; Shen, W. Forced wetting and dewetting of liquids on solid surface and their roles in offset printing. *Colloids and surfaces A: Physicochemical and engineering aspects* **2008**, 316, 62-69.
- (8) Yuan, J. J.; Yan, S. Y.; Zhang, X. Superhydrophilic antifogging broadband antireflective coatings with worm-like nanostructures fabricated by one dip-coating method and calcination. *Applied Surface Science* **2020**, 506, 144795.

- (9) Kavitha, M. K.; Rolland, L.; Johnson, L.; John, H.; Jayaraj, M. K. Visible light responsive superhydrophilic TiO₂/reduced graphene oxide coating by vacuum-assisted filtration and transfer method for self-cleaning application. *Materials Science in Semiconductor Processing* **2020**, 113, 105011.
- (10) Zisman, W.A. Relation of the equilibrium contact angle to liquid and solid constitution. *Contact Angle, Wettability, and Adhesion* **1964**, 43, 1-51.
- (11) Yeo, L. Wetting and spreading. *Encyclopedia of Microfluidics and Nanofluidics*, Li, D. Q., Eds.; Springer: Boston, 2008; pp 2186-2196.
- (12) Ye, X.M.; Zhang, X.S.; Li, M.L. Contact line dynamics of two-dimensional evaporating drops on heated surfaces with temperature-dependent wettabilities. *International Journal of Heat and Mass Transfer* **2019**, 128, 1263-1279.
- (13) Yang, X.M.; Zhong, Z.W. Asymmetric liquid wetting and spreading on surfaces with slanted micro-pillar arrays. *Soft Matter* **2013**, 9, 11113-11119.
- (14) Johnson, P.; Routledge, T. Wetting and spreading of commercially available aqueous surfactants on porous materials. *Colloids Interfaces* **2019**, 3, 14.
- (15) Tanaka, K.; Iwamoto, K. Effective shear displacement on lateral adhesion force of a liquid bridge between separated plates. *Tribology Letters* **2016**, 64.
- (16) Davoudi, M.; Amrei, M.M. Measurement of inflection angle and correlation of shape factor of barrel-shaped droplets on horizontal fibers. *Separation and Purification Technology* **2018**, 204, 127-132.

(17) Johnson, R. E.; Dettre, R. H. Wettability and contact angles. *Surface and Colloid Science*, Matijevic, E., Eds.; John Wiley & Sons Inc: New York, 1969; Vol. 2, pp 85-153.

(18) Allain, C.; Ausserre, D.; Rondelez, F. A new method for contact-angle measurements of sessile drops. *Journal of Colloid and Interface Science* **1985**, 107, 5-13.

(19) Fondecave, R.; Wyart, F. B. Polymers as dewetting agents. *Macromolecules* **1998**, 31, 9305-9315.

(20) Zheng, L.; Wang, Y. X. Effect of curvature, contact angle, and interfacial subcooling on contact line spreading in a microdrop in dropwise condensation. *Langmuir* **2002**, 18, 5170-5177.

(21) Gokhale, S. J.; Plawsky, J. L. Experimental investigation of contact angle, curvature, and contact line motion in dropwise condensation and evaporation. *Journal of Colloid and Interface Science* **2003**, 259, 354-366.

(22) Kariyasaki, A.; Yamasaki, Y. Measurement of liquid film thickness by a fringe method. *Heat Transfer Engineering* **2009**, 30, 28-36.

(23) Murakami, D.; Kobayashi, M.; Moriwaki, T.; Ikemoto, Y.; Jinnai, H. Spreading and structuring of water on superhydrophilic polyelectrolyte brush surfaces. *Langmuir* 2013, 29, 1148-1151.

(24) Hashimoto, S.; Hong, C. Transient growth process of precursor film at early stage of droplet spreading. *Journal of Thermal Science and Technology* **2012**, 7, 487-496.

(25) Mu, L.; Kondo, D. Sharp acceleration of a macroscopic contact line induced by a particle. *Journal of Fluid Mechanics* **2017**, 830, R1.

- (26) Hadjiiski, A.; Dimova, R.; Denkov, N. D.; etls. Film trapping technique: precise method for three-phase contact angle determination of solid and fluid particles of micrometer size. *Langmuir* **1996**, *12*, 6665-6675.
- (27) Hariharan, P. *Basics of interferometry*, Academic Press, London, 2010.
- (28) Silicone Division Sales and Marketing Department I; Silicone Fluid KF-96 Performance Test Results; Shin-Etsu Chemical Co., Ltd.: Tokyo, 2004.
- (29) Sakai, J. *Fundamentals of optical instruments*, Morikita Publishing Corporation: Tokyo, 2013; pp 90-91.
- (30) Born, M.; Wolf, E. *Principles of Optics*. New York, NY: Pergamon Press INC 1959; pp 37.
- (31) Joanny, J.F.; Gennes, de P.G. Upward creep of a wetting fluid : a scaling analysis. *Journal de Physique* **1986**, *47*, 121-127.
- (32) Heslot, F.; Fraysse, N.; Cazabat, A.M. Molecular layering in the spreading of wetting liquid drops. *Nature* **1989**, *338*, 640-642.
- (33) Popescu, M.N.; Oshanin, G.; Dietrich, S.; Cazabat, A.M. Precursor films in wetting phenomena. *Journal of Physics: Condensed Matter* **2012**, *24*, 243102.
- (34) Kavehpour, H.P.; Ovryn, B.; McKinley, G.H. Microscopic and macroscopic structure of the precursor layer in spreading viscous drops. *Physical Review Letters* **2003**, *91*, 196104.
- (35) Yuan, Y.H.; Lee, T.R. Contact angle and wetting properties. *Surface Science Techniques* **2013**, 3-34.